Sequence-specific fluorescence turn-on sensing of RNA by DNA probes incorporating the tricyclic cytidine analogue ^{DEA}tC

M. Benjamin Turner,[a,†] Julian M. Cizmic,[a,†] Dana B. Rosansky,[a] Jesús Ceja,[a] Marissa Patterson,[b] Scott Kilcoyne,[b] Kodi Thurber,[b] Grace Kim,[a] Tammy J. Dwyer,[b] and Byron W. Purse*

a) *Department of Chemistry and Biochemistry, San Diego State University, San Diego, CA 92182*

b) *Department of Chemistry and Biochemistry, University of San Diego, San Diego, CA 92110*

E-mail: bpurse@sdsu.edu

† equal contributions

ABSTRACT

Sequence-specific fluorescent probes for RNA are widely used in microscopy applications such as FISH and a growing number of newer approaches to live-cell RNA imaging. The sequence specificity of most of these approaches relies on differential hybridization of the probe to the correct target. Competing sequences with only one or two base mismatches are prone to causing off-target recognition. Here, we report the sequence-specific fluorescent detection of model RNA targets using a tricyclic cytidine analogue ^{DEA}tC that is included as a surrogate for natural cytidine in DNA probe strands and that reports directly on Watson–Crick base pairing. The ^{DEA}tC-containing DNA oligonucleotide probes exhibit an average 8-fold increase in fluorescent intensity when hybridized to matched RNA with ^{DEA}tC base paired with G, and little fluorescence turn-on when ^{DEA}tC is base paired with A. Duplex structure determination by NMR, time-resolved fluorescence studies and Stern–Volmer quenching experiments suggest that the combination of greater π stacking and narrower grooves in the A-form DNA–RNA heteroduplex provides additional shielding and favorable electronic interactions between bases, explaining why ^{DEA}tC's fluorescence turn-on response to RNA targets is typically three-fold greater than for DNA targets.

INTRODUCTION

Fluorescent labeling methods for RNA have many applications in tracking, locating, and quantifying RNA in fixed and living cells.[1–5] Metabolic labeling for RNA imaging can be performed using reactive nucleoside analogues such as 5-ethynyluridine and azido nucleosides, which can be click labeled following incorporation, or using intrinsically fluorescent nucleoside analogues for direct RNA imaging without staining.[3,6–10] Artificially induced uptake, trafficking and function of exogenously produced RNAs can be monitored by including minimally

perturbing fluorescent base analogues when these RNAs are prepared.[2,11] But the most widely used applications of fluorescent imaging in RNA biology involve the detection of specific target sequences in cells or tissues.

Fluorescent hybridization probes recognize target sequences by base pairing. They can either be designed such that excess probe must be washed away prior to imaging, or they can provide a fluorescent response specific to their targets. Fluorescence in situ hybridization (FISH) typically involves the displacement of a quencher from a fluorescently labeled oligonucleotide probe, giving a turn-on response.[1,12] Forced intercalation (FIT) probes are single-stranded nucleic acids or peptide nucleic acids with an intercalative fluorophore (e.g. thiazole orange) substituted for one nucleobase.[13,14] Upon duplex or triplex formation with single- or double-stranded targets, respectively, the fluorophore is induced to intercalate, greatly increasing its fluorescence. Molecular beacons are oligonucleotide hairpins with a fluorophore appended to one terminus and a quencher appended to the other.[15] They exhibit target-specific fluorescence turn-on upon hairpin opening, driven by the formation of a more stable hybrid duplex with the target. Fluorogenic aptamers are frequently used in place of fluorophores for RNA imaging in cells.[16–18] The aptamer's ability to exchange fluorogenic ligands overcomes the problem of photobleaching. CRISPR-based methods using catalytically inactive dCas13 can also be used to image endogenous RNAs using a guide RNA to provide target specificity.[19]

One of the most important limitations of these probing schemes is that their sequence-specificity is determined primarily by the relative affinity for a matched vs. mismatched RNA target. The greater stability of GC as compared with AT base pairs creates bias, and sequences with a single mismatch may have only slightly depressed binding affinity as compared with a perfectly matched complement. Accordingly, many of these probes are prone to false positives, especially in GC-rich sequences or in samples with a high abundance of off-target RNAs. An attractive alternative is to develop fluorescent probes that reported directly on RNA sequence by altering their fluorescence in response to base pairing.

Fluorescent nucleobase analogues (FBAs) are widely used in studies on the structure, dynamics, and biomolecular interactions of nucleic acids, and they have great potential to address the challenge of sequence-specific nucleic acid detection.[20–23] Because they can be present at the Watson–Crick interface, their fluorescence can report directly on the identity of the base pairing partner. Since the discovery of 2-aminopurine's (2AP) fluorescence in 1969,[24] more

than 100 fluorescent nucleoside analogues have been reported.[22] Intrinsically fluorescent nucleobase analogues have been used to report on local structure, conformation, and dynamics of nucleic acids, sequence (mis)matches, enzyme-mediated nucleobase modifications, and changes in local polarity or pH.[25–29] Some nucleobase analogues such as 2AP experience nearly complete emission quenching when base-stacked in double-stranded nucleic acids,[30–32] however others may remain emissive when base-stacked, [33–36] including the largely environmentally insensitive tricyclic cytidine (tC) nucleobase.[37] By expanding on the parent tC molecular scaffold with a series of chemical modifications to the original phenothiazine scaffold, we have developed novel derivatives with environmentally sensitive fluorescent properties.[25,34,38] One of these compounds, the tricyclic cytidine analogue ^{DEA}tC, is nearly non-emissive as a free nucleoside in aqueous solution (Φ_{em} = 0.006) but experiences up to a 20-fold fluorescence turn-on effect (up to Φ_{em} = 0.12) when base-stacked in double-stranded DNA (dsDNA) and base-paired with guanine (Figure 1), with some dependence on the identity of neighboring bases.[39] This fluorescence turn-on response to base pairing and stacking is rare; a few other base analogues that exhibit significant fluorescent increases in response to duplex formation have been reported and their turn-on results for local rigidification.[40,41]

Here, we investigate the fluorescence turn-on response of ^{DEA}tC to DNA–RNA heteroduplex formation, showing that its fluorescence increase is more than two-folder greater than in DNA–DNA homoduplex formation and with less sensitivity to the identity its base-stacked neighbors. NMR structure determine of a 10-mer dsDNA duplex including ^{DEA}tC shows that it extends into the major groove, but does not significantly perturb duplex structure. Time-resolved fluorescence measurements and Stern–Volmer quenching measurements indicate that the enhanced performance of ^{DEA}tC in DNA–RNA is attributable primarily to altered electronic interactions with stacked bases as compared with DNA–DNA, a consequence of the A-form conformation of the heteroduplex.

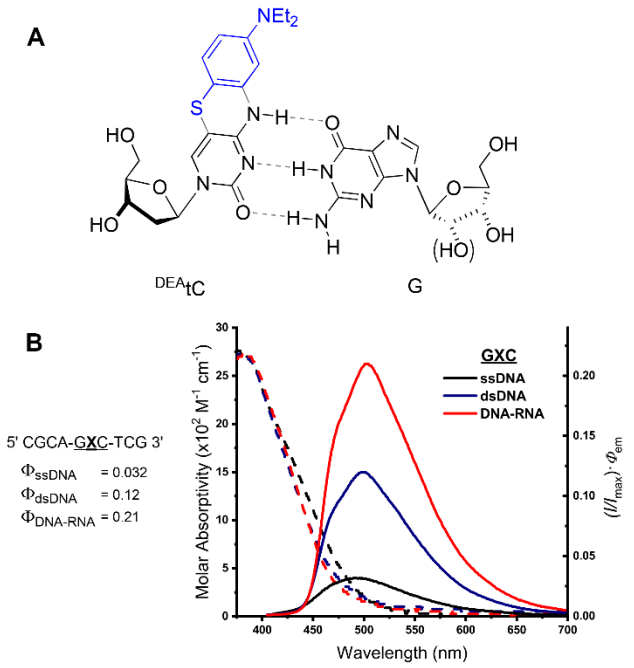

Figure 1. Structure and fluorescent properties of the ^{DEA}tC fluorescent nucleoside analogue. Absorption and emission spectra are shown for a 10-mer DNA strand containing an internal 5′ GXC 3′ sequence, where X is ^{DEA}tC. Fluorescence turn-on is observed upon hybridization with a DNA (blue) or RNA (red) complement. Fluorescence spectra are scaled to Φ_{em} at λ_{max}.

RESULTS

Synthesis of ^{DEA}tC and design and preparation of oligonucleotide probes

^{DEA}tC and its corresponding dimethoxytrityl-protected phosphoramidite were synthesized as reported previously.[25,42] To measure ^{DEA}tC's fluorescent properties in DNA–RNA heteroduplexes and compare with similar measurements in DNA–DNA homoduplexes,[42] we selected a set of eight 10-mer sequences with varied 3′- and 5′-neighboring nucleobases that we and others have used previously to study FBAs (Table 1). The ^{DEA}tC amidite was incorporated into these sequences using standard solid-phase synthesis conditions, except the coupling time for the ^{DEA}tC amidite was increased 10-fold. The identity and purity of the sequences was confirmed by mass spectrometry and HPLC (see SI). We named the sequences according to the identity of the 3′- and 5′-neighbors. For example, GXC refers to the sequence 3′-CGCAGXCTCG-5′, where X is ^{DEA}tC.

Fluorescence of ^{DEA}tC in single-stranded and duplex oligonucleotides

^{DEA}tC has low fluorescence as a free nucleoside, with an emission quantum yield Φ_{em} = 0.006 ($\lambda_{max,abs}$ = 395 nm and $\lambda_{max,em}$ = 493 nm) in 1× PBS buffer at pH 7.4. This fluorescence is

approximately two- to three-fold brighter when ^{DEA}tC is present in single-stranded DNA oligonucleotides (Figure 2 and Table S1).[42] A much greater increase in fluorescence, up to Φ_{em} = 0.12, occurs upon hybridization to a matched DNA complement, but not when ^{DEA}tC is mispaired with adenine or present opposite an abasic site (Table S2).[42] The magnitude of this Φ_{em} increase is influenced by the 3′- and 5′-neighbors of ^{DEA}tC. Some sequences, such as AXA, exhibit up to a 5-fold fluorescence increase upon hybridization to form a matched dsDNA duplex. In these sequences, the single-stranded ^{DEA}tC-containing oligonucleotide probe has especially low fluorescence. The brightest sequences have guanosine as the 5′-neighbor of ^{DEA}tC, but these exhibit only a 2- to 3-fold fluorescence turn-on upon matched hybridization.

Here, we measured the steady-state fluorescence of ^{DEA}tC in DNA–RNA heteroduplexes using the same 10-mer DNA oligonucleotide sequences by hybridized them to RNA complements. Consistently greater ^{DEA}tC fluorescence intensity is observed in the DNA–RNA duplexes, with GXC remaining the most emissive sequence and CXT the least (Table 1 and Figure 2). GXC exhibited the greatest Φ_{em} = 0.22, a 6.9-fold increase with respect to the GXC 10-mer ssDNA and a 37-fold increase with respect to the ^{DEA}tC nucleoside. Most other sequences had Φ_{em} values ranging from 0.10 – 0.17 (Table 1). CXT exhibited the lowest Φ_{em} = 0.048, but was still 2.4-fold brighter than the ssDNA probe strand prior to hybridization. The AXA sequence exhibits the largest fluorescence enhancement, a 14-fold increase with respect to the ^{DEA}tC-containing ssDNA oligo, upon hybridization with complementary RNA. CXA shows the largest difference in turn-on enhancement when hybridized to RNA as compared with DNA. Brightness [$B = \varepsilon \cdot \Phi$] is approximated using ε_{395} = 2,700 M^{-1} cm^{-1} for ^{DEA}tC, although the molar absorptivity of DNA bases usually decreases 25 – 40 % in oligonucleotides compared to free nucleoside monomers.[43] The exact decrease in ^{DEA}tC's absorptivity upon inclusion in an oligonucleotide has not been measured. The Stokes shifts among the heteroduplexes are largely consistent, ranging from 83 – 110 nm. The excitation energy as determined by $\lambda_{max,abs}$ ranges from 3.02–3.16 eV, which is very similar to the range from 2.94–3.12 eV observed for ^{DEA}tC in dsDNA.[42] These excitation energies are slightly lower than the range for parent tC, 3.11–3.19 eV in dsDNA.[33] The excitation energy of ^{DEA}tC as a free nucleoside is 3.14 eV. Similar excitation energies for ^{DEA}tC when base paired and stacked in a dsDNA or DNA–RNA indicates that the energy gap between the ground (S_0) and excited states (S_1) remains relatively constant.

The stability of the DNA–RNA heteroduplexes and some aspects conformational perturbation caused by ^{DEA}tC can be measured by ΔT_m, the difference in melting temperature between the ^{DEA}tC-containing and native duplexes (Table 1). Depending on the identity of the neighboring bases, ΔT_m varies between −7.0 °C (GXC) and +1.5 °C (CXT). In six out of the eight tested sequences, ^{DEA}tC is typically moderately destabilizing. The corresponding values for ^{DEA}tC-containing DNA–DNA homoduplexes are a range from −14.5 °C (GXC) to +6.7 °C (CXC). ^{DEA}tC is, on average, more destabilizing in DNA–DNA duplexes. This result could be considered surprising, given that DNA–RNA heteroduplexes take the A-form conformation, in contrast with B-form for DNA–DNA. The π system overlap in stacked neighboring bases is greater in the A-form. Circular dichroism measurements show that the A-form is retained in DNA–RNA and the B-form retained in DNA–DNA when ^{DEA}tC substitutes for one cytidine in the sequences studied here (Figure S6).

Table 1. Steady-State fluorescence measurements from ^{DEA}tC in DNA-RNA duplexes.

DNA Sequence (5′→3′)	$\lambda_{max, abs}$ (nm)	$\lambda_{max, em}$ (nm)	Stokes Shift (nm)	Φ_{em} (±)	ΔT_m (±)[a]	Brightness (M^{-1} cm^{-1})[b]
CGCA-**GXC**-TCG	404	504	100	0.22 (7.4x10^{-3})	-7.05 (0.77)	594
CGCA-**GXA**-TCG	394	501	107	0.17 (1.4 x10^{-2})	-2.83 (1.8)	459
CGCA-**TXA**-TCG	409	503	94	0.14 (2.4 x10^{-2})	+0.61 (0.60)	378
CGCA-**CXA**-TCG	410	497	87	0.13 (5.2 x10^{-2})	-3.39 (0.85)	351
CGCA-**CXC**-TCG	411	494	83	0.12 (3.9 x10^{-2})	-6.92 (0.64)	324
CGCA-**AXA**-TCG	392	502	110	0.11 (1.6x10^{-2})	-1.16 (1.0)	297
CGCA-**GXG**-TCG	402	503	101	0.10 (2.7 x10^{-4})	-5.43 (0.54)	270
CGCA-**CXT**-TCG	410	499	89	0.048 (6.9 x10^{-4})	+1.49 (1.1)	130

The position of ^{DEA}tC is denoted by X. Sequence names are bolded. Complementary RNA sequences are matched. *a)* Duplex stability is calculated by subtracting T_m (°C) of duplexes with natural cytidine from T_m (°C) of duplexes substituting ^{DEA}tC at position X. *b)* Brightness is calculated using ε = 2,700 M^{-1} cm^{-1} at 395 nm. Measurements were made in 1× PBS buffer at pH 7.4.

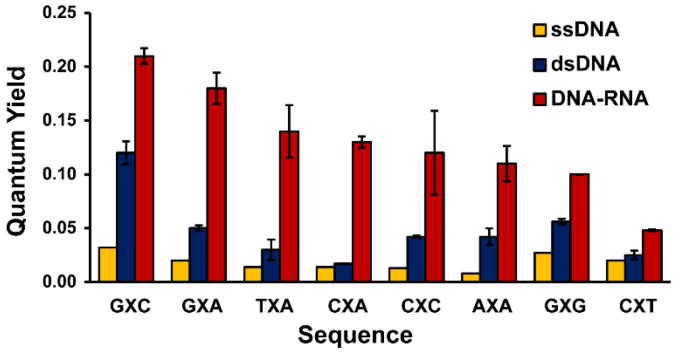

Figure 2. Fluorescence quantum yields of ^{DEA}tC-containing 10-mers. Sequence names are given in Table 1. ssDNA = ^{DEA}tC-containing 10mer as a single-stranded oligonucleotide. dsDNA refers to those ^{DEA}tC-containing 10mers hybridized to a complementary 10-mer DNA sequence. DNA–RNA refers to those ^{DEA}tC-containing 10-mers hybridized to a complementary 10-mer RNA sequence. Error bars indicate the standard deviation of the mean. For CXA dsDNA, CXC dsDNA, GXG dsDNA, GXG DNA–RNA, and CXT DNA–RNA standard deviations were < 2.5×10^{-3}. Measurements were made in 1× PBS buffer at pH 7.4.

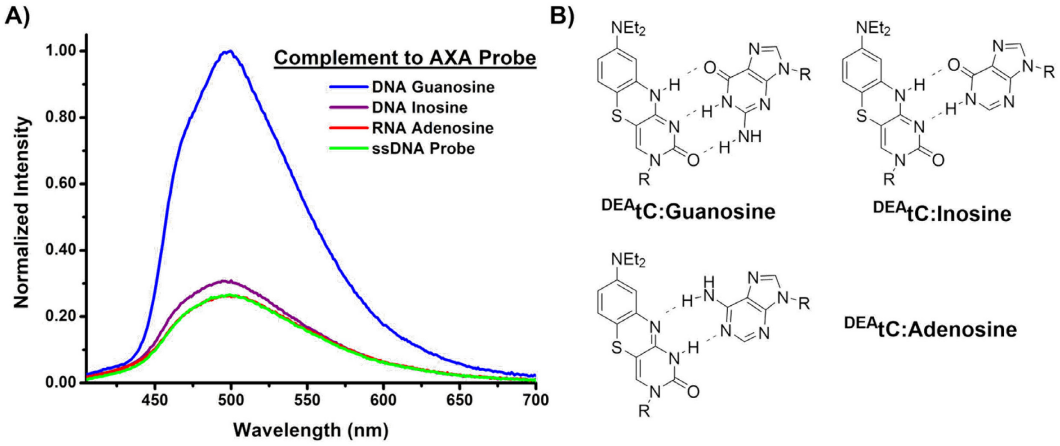

Figure 3. Fidelity of ^{DEA}tC's fluorescence turn-on. Fluorescent emission of the AXA probe strand hybridized to complementary DNA or RNA strands with ^{DEA}tC:G, ^{DEA}tC:I, and ^{DEA}tC:A pairings is shown. Emission intensity (Φ_{em}) is normalized to that of ^{DEA}tC:G in dsDNA. The normalized fluorescent intensity of the AXA probe strand is shown as a baseline for the absence of turn-on (green).

Our past studies on ^{DEA}tC in duplex DNA oligonucleotides show that its fluorescence turn-on is dependent on matched base pairing with guanine.[42] Opposite adenosine or an abasic site, ^{DEA}tC does not exhibit fluorescence turn-on. Consistent with that finding, ^{DEA}tC's fluorescence turn-on response to RNA is dependent on canonical Watson-Crick base-pairing with guanine. When the quantum yield was measured for a DNA-RNA ^{DEA}tC:A mismatch using the AXA sequence, the fluorescence was comparable to AXA ssDNA Φ_{em}, revealing no significant turn-on response (Figure 3A). We performed a similar fidelity experiment with a DNA complement that included the non-canonical nucleoside inosine (Figure 3B), which bears a hypoxanthine nucleobase. Inosine has a Watson-Crick hydrogen-bonding face partially resembling guanine and consequently base pairs with cytosine.[44] I:C base-pairs differ from classic G:C base pairs in that hypoxanthine engages in two hydrogen bonds with cytosine, lacking an H-bond with the *O2* acceptor on cytosine (Figure 3B). Although inosine presents similar features to guanosine, we did not observe a significant fluorescence turn-on for a dsDNA

^{DEA}tC:I duplex. Engaging the three Watson-Crick H-bonding sites on ^{DEA}tC with a contraposing guanine is required for induced fluorescence turn-on.

NMR-based duplex conformational studies

We performed NMR structure determination on a ^{DEA}tC-containing DNA–DNA duplex and the corresponding native duplex to further study changes in structure and dynamics induced by this analogue. For these experiments, we selected a modified GXC sequence, chosen both because it is the brightest sequence studied and it has the most perturbed melting temperature. To facilitate NMR structure determination, we slightly modified the sequence to 5′-CGTA-GXC-TCC-3′, which we will call GXC′ (X = ^{DEA}tC; c.f. the GXC sequence in Table 1). The altered sequence has 5′- and 3′-termini designed to minimize fraying, without changing ^{DEA}tC's closest neighboring bases. To verify that this sequence change does not significantly alter the fluorescence, we measured absorption and emission spectra of GXC′ and determined its Φ_{em} as a single-stranded oligo (Φ_{em} = 0.021), in a matched DNA–DNA duplex (^{DEA}tC base paired with G; Φ_{em} = 0.13), and in a DNA–DNA duplex with ^{DEA}tC base paired with A (Φ_{em} = 0.041). These values are nearly the same as those observed for GXC, and they show that "mispairing" ^{DEA}tC with A does not induce a large fluorescence turn-on in this alternative set of neighboring bases. Accordingly, ^{DEA}tC's local chemical environment in this modified duplex is effectively the same as in the parent GXC sequence.

Signal assignments of all exchangeable and non-exchangeable nucleic acid protons of the GCC′ (the native duplex corresponding to GXC′) and GXC′ duplexes (with the exception of C5′H and C5″H) were made based on standard procedures.[10-11] Imino N-H protons in the duplexes were visible at 27 °C (GCC′) and 15°C (GXC′). Figure 4 shows the sequential assignment of the aromatic base protons (H6/H8) and the C1'H of the DNA sequence in GCC′ (27°C) and GXC′ (15°C) in the NOESY spectrum collected in D_2O. Sequential connectivity was also observed for the aromatic protons with most of the C2′H and C2″H of the deoxyribose rings.

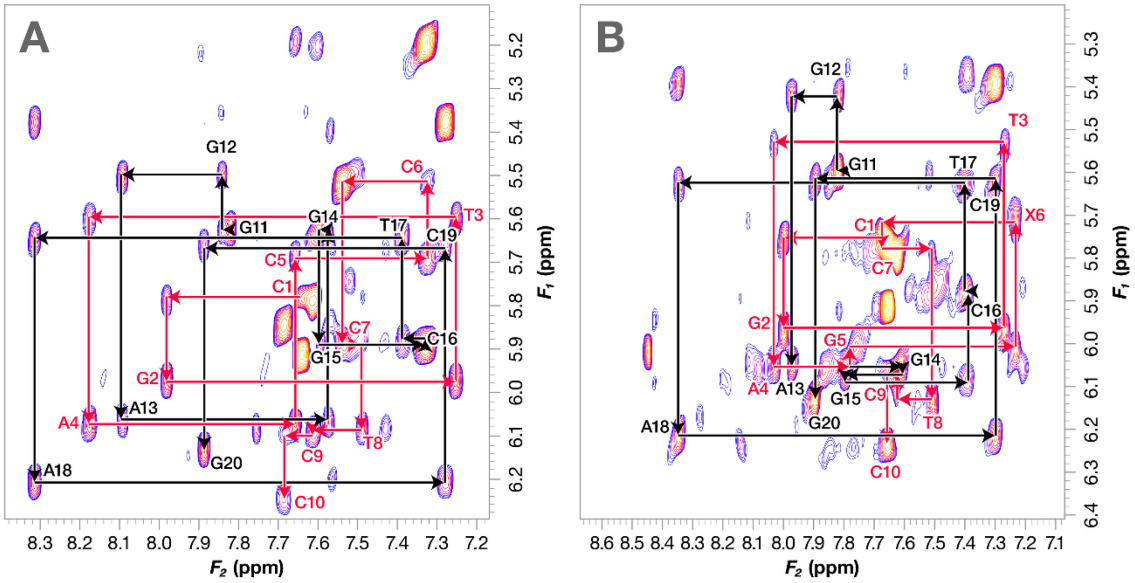

Figure 4. Deoxyribose H1′ to aromatic portion of the NOESY spectra of GCC′ (A) at 27ºC and GXC′ (B) at at 15ºC, both at a mixing time of 300 ms. The sequential connectivity for H1′ to H6/H8 for residues 1–10 is indicated by a red line, while that for residues 11–20 is indicated by a black line.

The families of structures used to represent each duplex were generated using statistical analysis modeled after Smith, *et al.*[12] The structures resulting from rMD for each duplex were randomly ordered and the mean all-atom pairwise rmsd was calculated for the first two structures, then the first three structures, etc. This process was repeated 500 times with each round using a different ordering of the structures. This analysis predicts the minimum number of structures necessary to fully represent the conformational space consistent with the experimental data. It was determined that 20 structures (GCC′) and 20 structures (GXC′) were sufficient to describe the duplexes. The structures in each family were chosen to minimize the molecular mechanics (AMBER) energy and the constraint violation energy. The superposition of the family of structures describing both duplexes is shown in Figure 5 along with the average structures for the duplexes and the binding sites.

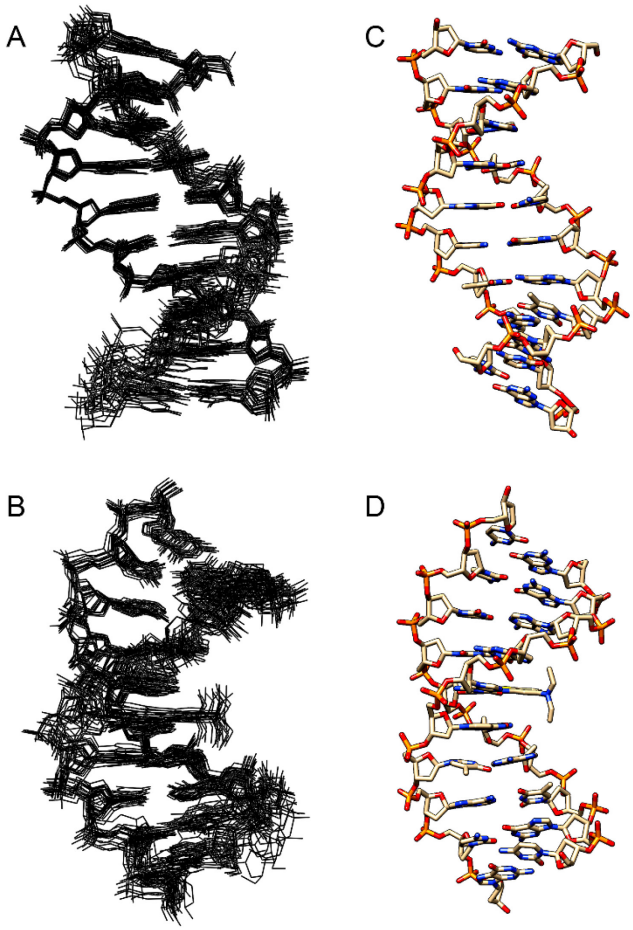

Figure 5. Superposition of family of 20 structures describing the GCC′ duplex (A) obtained by rMD; superposition of the family of 20 structures describing the GXC′ duplex (B) obtained by rMD, and a comparison of the average structures for GCC′ (C) and GXC′ (D).

The energy and rmsd characteristics of the ensembles of structures for GCC′ and GXC′ are summarized in Table 2. The data indicate structural convergence for the GCC′ duplex with a rmsd of 1.02 Å (rms difference from the mean structure of 0.70 Å) and for the GXC′ duplex with a rmsd of 1.27 Å (rms difference from the mean structure of 0.88 Å), given that the starting structures for both duplexes represented a range of B-DNA conformations with initial rmsd values of 3.97 Å (GCC′) and 3.98 Å (GXC′). The final collection of structures has a total restraint violation summing to 7.6 ± 0.4 kcal for GCC′ and 6.0 ± 0.7 kcal for GXC′, amounting to 0.2% (GCC′) and 0.1% (GXC′) of the total energy of each system.

Table 2. Summary of energies, rmsd values and violations for ensembles of structures.

Molecular Mechanics energies (kcal):	GCC′	GXC′
E_{Amber}	-4493.3 ± 1.0	-4476.9 ± 1.6
E_{viol}	7.6 ± 0.4	6.0 ± 0.7
Average Pairwise rmds (Å):		
DNA	1.02	1.27
Distance violations (Å):		
$0.05 < d \leq 0.10$	5	9
$0.10 < d \leq 0.20$	0	2
$0.20 \leq d$	0	0

Helical analyses (Figures S9–S11) using Curves5+ indicate that both GCC′ and GXC′ duplexes exhibit overall B-form DNA geometry. In the region of the ^{DEA}tC moiety there is no major disruption in the GXC′ duplex relative to the unmodified GCC′. There are minor differences in a few helical parameters such as roll, shift, stagger, tip, and *y*-displacement likely due to dynamic motion as the duplex accommodates the diethylamino group in the major groove. Relative to the GCC′ duplex, the GXC′ duplex is more highly dynamic, as evidenced by the loss of signal (due to broadening) in key regions of the NOESY spectra including NOEs between protons on the DNA and the CH_3 of the diethylamino groups on ^{DEA}tC. These particular NOEs broaden but are visible at 10°C (presumably from aggregation of the duplex – not unusual), sharp at 15 °C, weakening at 20°, and not visible at 25° and 35°C. The observed increase in duplex dynamics when ^{DEA}tC substitutes for C in this sequence explains the lower melting temperature of GXC. We note that the diethylamino group of ^{DEA}tC is electron-donating and guanine is the most electron-rich canonical nucleobase. We propose that the forced π stacking of these electron-rich arenes upon duplex formation is destabilizing and drives the increased dynamics.

Time-resolved fluorescence measurements

To gain further insight into the origins of ^{DEA}tC's fluorescence turn-on response to matched RNA, we performed time-resolved fluorescence spectroscopy using time-correlated single photon counting (TCSPC) to measure the excited-state lifetimes τ (Figure S1–S3 and Table 3). These measurements were performed using a Delta Pro™ Fluorescence Lifetime System (Horiba Scientific) with a LED Delta Diode 371 nm excitation source, with samples

dissolved in in 1× PBS buffer at pH 7.4. Data fitting to determine fluorescence lifetimes was performed using the maximum entropy method as implemented in the MemExp software (ver. 6.0).[45,46] We calculated amplitude average fluorescence lifetimes <τ> and the radiative and nonradiative rate constants for relaxation, k_f and k_{nr}, respectively.[39]

In most observed contexts, the ^{DEA}tC nucleoside's excited state exhibits biexponential decay. The major component of this decay function has a lifetime τ = 7.3 ns for the free nucleoside, and this lifetime increases to τ ≈ 10 ns in DNA–RNA duplexes. A shorter lifetime of τ ≈ 2 ns is observed in most duplexes as a minor component. The amplitude average fluorescence lifetime <τ> ranges from 6.3–10.5 ns for the duplexes and is not clearly correlated with any one fluorescence property such as Φ_{em}. Traditionally, a biexponential decay is interpreted to result from the fluorophore being present in two distinct environments. While it is not certain what those environments might be in this context, at least for these matched base pairs, one possibility is that an imino tautomer of ^{DEA}tC, which would be expected to be a minor component, could form a wobble base pair with G. Another possibility is that sequences exhibiting τ_2 have a minor conformer giving rise to this component. While these results do not clearly explain the origin of ^{DEA}tC's fluorescence turn-on effect, we do note that the lifetime of the major component increases from 7.3 to approximately 10 ns in the duplex, indicative of an environment that slows excited state relaxation (i.e. limits quenching).

To further shed light on ^{DEA}tC's fluorescence turn-on, we performed additional TCSPC measurements with ^{DEA}tC base paired with inosine and adenosine, respectively. Here, we observed a large increase in the contribution of a short lifetime $\tau_2 \approx 2$ ns in a biexponential decay (Figure 6). For these "mispairings", the short lifetime has an amplitude of 0.74 and 0.81, respectively. In contrast, the amplitude of the short lifetime $\tau_2 \approx 2$ ns was typically close to 0.3 in the "matched" sequences (i.e. those with ^{DEA}tC:G base pairs); here, the long lifetime dominates. These results show that both the ^{DEA}tC:I and ^{DEA}tC:A base pairs are associated with major populations of ^{DEA}tC in environments conducive to rapid quenching.

Table 3. Time-resolved fluorescence measurements of DEAtC nucleoside in DNA–RNA duplexes.

Sequence	Φ_{em}	τ_1 (ns)	α_1	τ_2 (ns)	α_2	$\langle\tau\rangle$ (ns)[a]	k_f (x10^7 s^{-1})[b]	k_{nr} (x10^7 s^{-1})[c]
Nucleoside	0.006	7.3	0.62	3.0	0.38	5.69	0.001	0.18
GXC	0.22	10.5	1.00	–	–	10.54	0.021	0.07
GXA	0.17	10.3	0.79	2.7	0.21	8.70	0.020	0.10
TXA	0.14	10.0	0.71	2.2	0.29	7.74	0.018	0.11
CXA	0.13	10.6	0.55	1.1	0.45	6.30	0.021	0.14
CXC	0.12	11.2	0.77	1.6	0.23	9.05	0.013	0.10
AXA	0.11	10.2	0.79	2.3	0.21	8.52	0.013	0.10
GXG	0.10	10.2	1.00	–	–	10.20	0.010	0.09
CXT	0.048	10.5	0.70	2.3	0.30	8.06	0.006	0.12
AXA†	n.d.	8.5	0.19	2.2	0.81	3.37		
AXA‡	n.d.	9.7	0.26	2.2	0.74	4.20		

Time-resolved measurements were performed using TCSPC and λ_{ex} = 371 nm. Sequences names are defined in Table 1. A single-component model were used for GXC and GXG because there was no clear evidence for a significant shorter-lifetime component. †hybridized to a complementary RNA strand with ^{DEA}tC base paired with adenosine. ‡hybridized to a complementary DNA strand with ^{DEA}tC base paired with inosine. *a*) Amplitude average fluorescence lifetime $\langle\tau\rangle = \Sigma\alpha_i\tau_i$. *b*) Radiative decay rate is calculated as Φ_{em} divided by $\langle\tau\rangle$. *c*) Non-radiative decay rates were calculated using the equation $k_{nr} = (k_f/\Phi_{em}) - k_f$. n.d. = not determined

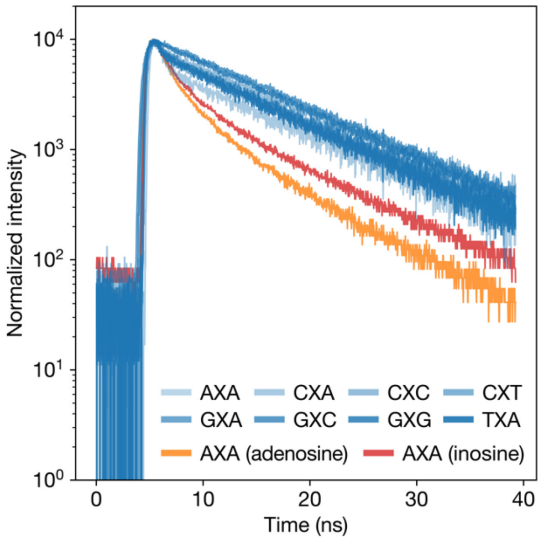

Figure 6. Time-resolved emission decays of various probes with ^{DEA}tC:G basepairs (blue lines) along with mispairings of the AXA probe with ^{DEA}tC:A (orange line) and ^{DEA}tC:I (red line).

Stern–Volmer studies on sensitivity to external quenchers

The general trends of ^{DEA}tC's brightness as depending on neighboring bases are similar in dsDNA and DNA–RNA duplexes, but the brightness is considerably greater in the latter. DNA–RNA hybrids typically adopt A-form conformation, similarly to dsRNA, which are structurally distinct from B-form.[47] CD spectroscopy revealed that all of the ^{DEA}tC-containing sequences adopted the A-form when paired to their complementary 10-mer RNA (Figure S6). These comparisons were performed by examining the CD spectral differences between sequences containing ^{DEA}tC to those containing natural cytosine and confirming the presence of a sharp transition at 210 nm.[48] One possible explanation for ^{DEA}tC's greater brightness in DNA–RNA is reduced accessibility to external quenchers in the deeper but narrower major groove of the A-form conformation. A-form has a greater tilt of the base-pair plane with respect to the central helical axis, approximately 11 base pairs per turn instead of 10 in B-form, and a greater extent of base stacking. The increased overlap of the bases and narrower major groove can be expected to endow greater shielding to the nucleobases from external quenchers in DNA–RNA. We tested this hypothesis by performing Stern–Volmer quenching analysis using chloride and iodide, which are commonly used collisional quenchers.

Stern–Volmer quenching experiments were performed with three sequences and two halide ions in sodium phosphate buffer (Figure 7; experimental details are provided in the Supporting Information). The two halides, chloride and iodide, differ in their ionic radius as well as their quenching potency, which has been correlated to their ionization energies.[49] Chloride has ionic diameter of about 334 pm while iodide has an ionic diameter of approximately 412 pm and is a stronger quencher.[50–52] Experiments were performed using the DNA–RNA oligonucleotides GXC, TXA, and CXA (Figures 4 and S8, and Table 4). GXC was the brightest sequence observed while TXA and CXA showed the most pronounced fluorescence increase in A-form DNA–RNA duplexes relative to fluorescence in B-form dsDNA. Using the recorded amplitude average fluorescence lifetimes and Stern–Volmer quenching coefficients, we calculated the bimolecular quenching rate constants k_q for the TXA and CXA sequences, comparing DNA–RNA with DNA–DNA. The results are that rate constants for quenching are greater for iodide, as expected, and that the rate constants for quenching are slower in the DNA–RNA duplexes. The difference is modest for the TXA sequence, only 5% slower quenching in DNA–RNA with chloride and 19% slower with iodine. The difference is much more in the CXA duplex, 53%

slower with chloride and 43% slower iodide. While significant, we note that ^{DEA}tC's fluorescence turn-on upon matched duplex formation is 5-fold greater in DNA–RNA than in DNA–DNA in the TXA sequence, and 9-fold greater in CXA. Accordingly, less sensitivity to quenching by solutes in DNA–RNA contributes to ^{DEA}tC's greater fluorescence turn-on, but it is not the most important effect.

Table 4. Quenching efficiency measured by Stern-Volmer analysis

		NaCl		NaI	
Sequence	**Duplex**	**K_{SV} ($x10^{-3}$ M^{-1}**	**k_q ($x10^8$ M^{-1} s^{-1})[a]**	**K_{SV} ($x10^{-3}$ M^{-1}, ±)**	**k_q ($x10^8$ M^{-1} s^{-1})[a]**
GXC	dsDNA	3.22 ±0.13	n.d.	3.22 ±0.23	n.d.
	DNA-RNA	2.23 ±0.072	2.12	2.63 ±0.92	2.49
TXA	dsDNA	1.46 ±0.072	2.11	3.63 ±0.14	5.24
	DNA-RNA	1.54 ±0.076	1.99	3.28 ±0.38	4.24
CXA	dsDNA	2.02 ±0.090	6.18	2.93 ±0.18	8.96
	DNA-RNA	1.84 ±0.057	2.92	3.22 ±0.10	5.11

The Stern–Volmer quenching constant is graphically measured. *a*) The bimolecular quenching constant (k_q) is calculated from the relation $K_{SV} = k_q\tau$.

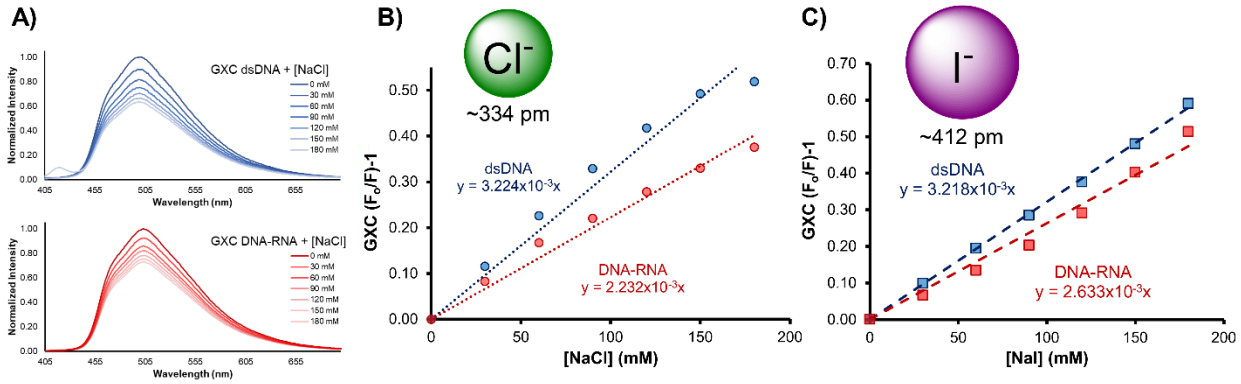

Figure 7. Stern-Volmer analysis of GXC duplexes. **A**) Fluorescence was measured as a function of [*Q*] and integration of emission spectra enabled graphical determination of Stern-Volmer quenching coefficients. **B)** Attenuated emission was recorded with varying [NaCl], and **C)** [NaI].

DISCUSSION

The fluorescence of most FBAs is quenched in the base stack by photoinduced electron transfer with neighboring bases, but in the last twenty years, a number of FBAs were introduce that retain robust fluorescence emission upon incorporation into duplex nucleic acids, with little sensitivity to base pairing and stacking. More recently, some of the first FBAs have been reported that provide substantial fluorescence increases in response to specific base pairing and stacking

interactions. These include ^{DEA}tC, for which we first reported a fluorescence turn-on responses to matched DNA, and ^{ts}T, a brightly fluorescent thymidine analogue with 5-fold fluorescence turn-on response that is specific for matched base pairing the adenosine in DNA–DNA duplexes. It is known that FBAs must have HOMO and LUMO energy levels the lie within the HOMO–LUMO gap of canonical nucleobases to avoid quenching by PET, but details of the mechanisms for fluorescence turn-on responses of these FBAs remain poorly understood, especially when those responses are specific to base pairing partners. These mechanisms of fluorescence turn-on are important for designing oligonucleotide probes for applications in biochemistry and biophysics and for the design of new nucleoside turn-on probes with complementary properties.

We previously published that ^{DEA}tC derivative is nearly non-emissive as a free nucleoside in aqueous solution but experiences up to a 20-fold fluorescence turn-on effect when base-stacked in double-stranded DNA (dsDNA) and base-paired with guanine. Using solvent isotope effects, we presented evidence that a substantial contributor to ^{DEA}tC's fluorescence turn-on is the ability of the duplex, specifically including Watson–Crick base pairing, to shield ^{DEA}tC from excited-state proton transfer. In the present study, we investigated how ^{DEA}tC's fluorescence turn-on in DNA–RNA duplexes compares with its response in DNA–DNA duplexes and which structural features might explain any observed differences.

Our steady-state fluorescence measurements show that ^{DEA}tC's fluorescence turn-on response in DNA–RNA duplexes is approximately twice as great as in DNA–DNA duplexes, is less sensitive to the identity of neighboring bases, and retains its specificity for base pairing with adenosine. While this large fluorescence turn-on effect, up to approximately 10-fold as compared with the single strand containing ^{DEA}tC or up to 35-fold as compared with the ^{DEA}tC nucleoside, has much potential utility as an bioanalytical tool, in this study we focused on investigating the fluorescence enhancement. We first sought to determine the extent to which ^{DEA}tC perturbs duplex structure. Differences in melting temperature ΔT_m show that ^{DEA}tC is typically, but not always, moderately destabilizing, particularly in the brightest sequence, GXC. It is less destabilizing than in dsDNA. As we observed previously in dsDNA, CD spectra show that ^{DEA}tC's presence in the DNA–RNA heteroduplex does not change the A-form conformation.

To further gain structural insight into the effects of ^{DEA}tC's presence, we used NMR to determine the conformation of a 10-mer dsDNA duplex GXC′ containing ^{DEA}tC a base pair with G, and compared it with conformation of the canonical duplex GCC′ determined similarly. As

anticipated from CD spectra, ^{DEA}tC does not significantly change the B-form conformation of dsDNA, but the duplex is significantly more dynamic at the site of the ^{DEA}tC:G base pair, as evident from the broadness of the NOESY signals. These enhanced dynamics are associated with lower duplex stability, which is corroborated by the lower T_m when ^{DEA}tC is present. The NMR structure shows that, on average, ^{DEA}tC base pairs and stacks similarly to cytosine, but with some of its additional arene structure and diethylamino group extending into the major groove, where it is exposed to water and solutes, constrained by the major groove structure.

The classic double-stranded structure of b-form DNA arises from the hydrophobic effect and π–π dispersion energies ($E_{\pi\text{-}\pi}$) between stacked nucleobases, with the fidelity of hydrogen bonding being the determinant of matched base pairing.[53–55] In canonical B-form DNA the observed twist angle (ω) is 36° offset from exact parallel alignment ($\omega = 0°$), whereas in A-form DNA the twist between consecutive base-pairs is smaller at $\omega = 33°$.[47] Increasing ω in B-form DNA was computationally shown to increase overall duplex thermodynamic stability, principally by reducing Pauli repulsion between neighboring bases.[56] In DNA–RNA A-form hybrids with greater base-pair overlap and reduced physical distance between base pairs, ^{DEA}tC should experience greater π–π interactions that may contribute to an increased fluorescence response. Another likely significant factor is that the polarity in A-form major grooves is predicted to mimic the polarity of 20% H_2O in 1,4-dioxane, about half the estimated polarity of B-form.[57] This less polar environment likely contributes to ^{DEA}tC's enhanced fluorescence.

To better understand how local structure in duplex nucleic acids influences radiative and nonradiative relaxation of ^{DEA}tC's excited state, we performed TCSPC studies on the free nucleoside and the duplexes. In most contexts, ^{DEA}tC exhibits biexponential decay, indicative of two populations. One population has a longer excited state lifetime $\tau \approx 7–10$ ns, and the second population has a shorter lifetime $\tau \approx 2$ ns. The population with the longer lifetime is dominant in all cases, except when ^{DEA}tC is "mispaired" with adenine or inosine, in which case the shorter lifetime is dominant. This change to a dominant shorter lifetime explains the lack of fluorescence turn-on response to these base pairings. While we do not have sufficient data to make rigorous structural assignments for these populations, we speculate that the shorter lifetime population may represent (i) a solvated state prone to ESPT quenching that is prevented by Watson–Crick base pairing *with three hydrogen bonds*, (ii) a tautomeric base pair in the case of ^{DEA}tC:A, or a combination of (i) and (ii) when ^{DEA}tC is base paired with A.

Last, we performed Stern–Volmer quenching studies to assess how differences in the A-form conformation might leave ^{DEA}tC less exposed to exogeneous quenchers. In addition to a more compressed helix, the A-form duplex as observed in DNA–RNA has deeper major grooves than that of B-form dsDNA.[47] While the major and minor grooves in B-form DNA have isometric depths, the narrower, deeper major grooves of A-form DNA–RNA restrict access and mobility of solvent molecules and some ions. Indeed, quenching rate constants determined from Stern–Volmer analysis and time-resolved fluorescence studies show that quenching by both chloride and iodide is slower in DNA–RNA, although the magnitude of the difference is sequence dependent. This finding supports the premise that reduced access to exogeneous quenchers by virtue of the narrower major groove in the DNA–RNA heteroduplex contributes to ^{DEA}tC's brighter fluorescence in this environment.

CONCLUSION

In this work, we sought to evaluate the fluorescence turn-on response of DNA strands incorporating ^{DEA}tC upon hybridization to complementary and mismatched RNA. Steady-state fluorescence measurements show that ^{DEA}tC's fluorescence turn-on response to matched RNA oligos is, on average, an 8-fold increase. This response is approximately triple the magnitude of increase upon hybridization with complementary DNA, and is dependent on the formation of a "matched" ^{DEA}tC:G base pair. Neighboring bases influence the extent of fluorescence turn-on, but to a lesser degree than is observed when fluorescence turn-on is induced by hybridization to complementary DNA. ^{DEA}tC is, in most sequences, modestly destabilizing, as indicated by depressed melting temperatures, but CD spectroscopy and NMR structure determination show that it does not significantly disrupt native B- and A-form conformations for DNA–DNA and DNA–RNA duplexes, respectively. In the most destabilized sequence context, GXC, NOESY signals indicate that the ^{DEA}tC:G base pair is more dynamic than a canonical C:G base pair. Time-resolved fluorescence studies show that "mispairing" ^{DEA}tC with A or I results in a substantial decrease in fluorescence lifetime $<\tau>$ by populating a state that is prone to quenching. Desolvation of ^{DEA}tC in the base stack and canonical Watson–Crick base pairing is required to minimize this quenching, and results in the fluorescence turn-on. Structural analysis of the A-form in comparison with the B-form and the determination of quenching rate constants by Stern–Volmer analysis and time-resolved fluorescence shows that the compacted A-form duplex, with

its narrower major groove structure, provides a less polar environment for ^{DEA}tC, with enhanced base stacking, and reduced access to soluble quenchers. These features together explain ^{DEA}tC's enhanced performance at fluorescence turn-on sensing of matched RNA sequences as compared with matched DNA sequences. Future work is needed to better understand how the electronic and hydrogen bonding interactions between stacked and paired nucleobase analogues gives rise to this and other fluorescent response to local environment in nucleic acids. Given the many advantages of fluorescence turn-on sensing over turn-off sensing, we look forward to many future applications of ^{DEA}tC in biophysical studies and as a fluorescent probe for specific target nucleic acid sequences. The latter application will necessitate the use of longer probe sequences such as 20-mers to enable target specificity in complex biological samples, and it is expected that attention will be needed to avoid probe designs that form stable hairpins or homodimers, which would increase background fluorescence. These studies will be the subject of future reports.

SUPPORTING INFORMATION

experimental details, materials, and methods, time-resolved fluorescence decay plots, data tables, data fitting methods, CD spectra and melting curves, Stern–Volmer plots, NMR spectroscopy and a description of methods used for molecular dynamics studies

ACKNOWLEDGEMENTS

This material is based upon work supported by the National Science Foundation under Grant Nos. (NSF CHE-1800529 and CHE-2102642) to B.W.P. The authors also thank San Diego State University and the University of San Diego for financial support and Peter Steinbach for helpful advice on the use of MemExp to fit time-resolved fluorescence data.

REFERENCES

(1) Cui, C.; Shu, W.; Li, P. Fluorescence in Situ Hybridization: Cell-Based Genetic Diagnostic and Research Applications. *Front. Cell Dev. Biol.* **2016**, *4* (SEP), 89. https://doi.org/10.3389/fcell.2016.00089.

(2) Baladi, T.; Nilsson, J. R.; Gallud, A.; Celauro, E.; Gasse, C.; Levi-Acobas, F.; Sarac, I.; Hollenstein, M. R.; Dahlén, A.; Esbjörner, E. K.; Wilhelmsson, L. M. Stealth Fluorescence

Labeling for Live Microscopy Imaging of MRNA Delivery. *J. Am. Chem. Soc.* **2021**, *143* (14), 5413–5424. https://doi.org/10.1021/jacs.1c00014.
(3) Wang, D.; Shalamberidze, A.; Arguello, A. E.; Purse, B. W.; Kleiner, R. E. Live-Cell RNA Imaging with Metabolically Incorporated Fluorescent Nucleosides. *J. Am. Chem. Soc.* **2022**, *144* (32), 14647–14656. https://doi.org/10.1021/jacs.2c04142.
(4) Le, P.; Ahmed, N.; Yeo, G. W. Illuminating RNA Biology through Imaging. *Nat. Cell Biol.* **2022**, *24* (6), 815–824. https://doi.org/10.1038/s41556-022-00933-9.
(5) Braselmann, E.; Rathbun, C.; Richards, E. M.; Palmer, A. E. Illuminating RNA Biology: Tools for Imaging RNA in Live Mammalian Cells. *Spec. Issue Chem. Tools Biol. Discov.* **2020**, *27* (8), 891–903. https://doi.org/10.1016/j.chembiol.2020.06.010.
(6) Jao, C. Y.; Salic, A. Exploring RNA Transcription and Turnover in Vivo by Using Click Chemistry. *Proc. Natl. Acad. Sci.* **2008**, *105* (41), 15779–15784. https://doi.org/10.1073/pnas.0808480105.
(7) Grammel, M.; Hang, H.; Conrad, N. K. Chemical Reporters for Monitoring RNA Synthesis and Poly(A) Tail Dynamics. *ChemBioChem* **2012**, *13* (8), 1112–1115. https://doi.org/10.1002/cbic.201200091.
(8) Sawant, A. A.; Tanpure, A. A.; Mukherjee, P. P.; Athavale, S.; Kelkar, A.; Galande, S.; Srivatsan, S. G. A Versatile Toolbox for Posttranscriptional Chemical Labeling and Imaging of RNA. *Nucleic Acids Res.* **2015**, *44* (2), e16. https://doi.org/10.1093/nar/gkv903.
(9) Sawant, A. A.; Galande, S.; Srivatsan, S. G. Imaging Newly Transcribed RNA in Cells by Using a Clickable Azide-Modified UTP Analog. In *RNA Detection: Methods and Protocols*; Gaspar, I., Ed.; Methods in Molecular Biology; Springer: New York, NY, 2018; pp 359–371. https://doi.org/10.1007/978-1-4939-7213-5_24.
(10) Fantoni, N. Z.; El-Sagheer, A. H.; Brown, T. A Hitchhiker's Guide to Click-Chemistry with Nucleic Acids. *Chem. Rev.* **2021**, *121* (12), 7122–7154. https://doi.org/10.1021/acs.chemrev.0c00928.
(11) Wahba, A. S.; Azizi, F.; Deleavey, G. F.; Brown, C.; Robert, F.; Carrier, M.; Kalota, A.; Gewirtz, A. M.; Pelletier, J.; Hudson, R. H. E.; Damha, M. J. Phenylpyrrolocytosine as an Unobtrusive Base Modification for Monitoring Activity and Cellular Trafficking of SiRNA. *ACS Chem. Biol.* **2011**, *6* (9), 912–919. https://doi.org/10.1021/cb200070k.
(12) Levsky, J. M.; Singer, R. H. Fluorescence in Situ Hybridization: Past, Present and Future. *J. Cell Sci.* **2003**, *116* (Pt 14), 2833–2838. https://doi.org/10.1242/jcs.00633.
(13) Hövelmann, F.; Gaspar, I.; Chamiolo, J.; Kasper, M.; Steffen, J.; Ephrussi, A.; Seitz, O. LNA-Enhanced DNA FIT-Probes for Multicolour RNA Imaging. *Chem Sci* **2016**, *7* (1), 128–135. https://doi.org/10.1039/C5SC03053F.
(14) Yoshino, Y.; Sato, Y.; Nishizawa, S. Deep-Red Light-up Signaling of Benzo[c,d]Indole–Quinoline Monomethine Cyanine for Imaging of Nucleolar RNA in Living Cells and for Sequence-Selective RNA Analysis. *Anal. Chem.* **2019**, *91* (22), 14254–14260. https://doi.org/10.1021/acs.analchem.9b01997.
(15) Monroy-Contreras, R.; Vaca, L. Molecular Beacons: Powerful Tools for Imaging RNA in Living Cells. *J. Nucleic Acids* **2011**, *2011*, 741723. https://doi.org/10.4061/2011/741723.
(16) Chen, X.; Zhang, D.; Su, N.; Bao, B.; Xie, X.; Zuo, F.; Yang, L.; Wang, H.; Jiang, L.; Lin, Q.; Fang, M.; Li, N.; Hua, X.; Chen, Z.; Bao, C.; Xu, J.; Du, W.; Zhang, L.; Zhao, Y.; Zhu, L.; Loscalzo, J.; Yang, Y. Visualizing RNA Dynamics in Live Cells with Bright and Stable Fluorescent RNAs. *Nat. Biotechnol.* **2019**, *37* (11), 1287–1293. https://doi.org/10.1038/s41587-019-0249-1.

(17) Cawte, A. D.; Unrau, P. J.; Rueda, D. S. Live Cell Imaging of Single RNA Molecules with Fluorogenic Mango II Arrays. *Nat. Commun.* **2020**, *11* (1), 1283. https://doi.org/10.1038/s41467-020-14932-7.
(18) Dolgosheina, E. V.; Jeng, S. C. Y.; Panchapakesan, S. S. S.; Cojocaru, R.; Chen, P. S. K.; Wilson, P. D.; Hawkins, N.; Wiggins, P. A.; Unrau, P. J. RNA Mango Aptamer-Fluorophore: A Bright, High-Affinity Complex for RNA Labeling and Tracking. *ACS Chem. Biol.* **2014**, *9* (10), 2412–2420. https://doi.org/10.1021/cb500499x.
(19) Tang, H.; Peng, J.; Peng, S.; Wang, Q.; Jiang, X.; Xue, X.; Tao, Y.; Xiang, L.; Ji, Q.; Liu, S.-M.; Weng, X.; Zhou, X. Live-Cell RNA Imaging Using the CRISPR-DCas13 System with Modified SgRNAs Appended with Fluorescent RNA Aptamers. *Chem. Sci.* **2022**, *13* (47), 14032–14040. https://doi.org/10.1039/D2SC04656C.
(20) Wilhelmsson, L. M. Fluorescent Nucleic Acid Base Analogues. *Q. Rev. Biophys.* **2010**, *43* (02), 159–183.
(21) Sinkeldam, R. W.; Greco, N. J.; Tor, Y. Fluorescent Analogs of Biomolecular Building Blocks: Design, Properties, and Applications. *Chem. Rev.* **2010**, *110* (5), 2579–2619.
(22) Xu, W.; Chan, K. M.; Kool, E. T. Fluorescent Nucleobases as Tools for Studying DNA and RNA. *Nat. Chem.* **2017**, *9* (11), 1043–1055. https://doi.org/10.1038/nchem.2859.
(23) Michel, B. Y.; Dziuba, D.; Benhida, R.; Demchenko, A. P.; Burger, A. Probing of Nucleic Acid Structures, Dynamics, and Interactions With Environment-Sensitive Fluorescent Labels. *Front. Chem.* **2020**, *8*, 112. https://doi.org/10.3389/fchem.2020.00112.
(24) Ward, D. C.; Reich, E.; Stryer, L. Fluorescence Studies of Nucleotides and Polynucleotides. I. Formycin, 2-Aminopurine Riboside, 2,6-Diaminopurine Riboside, and Their Derivatives. *J Biol Chem* **1969**, *244* (5), 1228–1237.
(25) Teppang, K. L.; Lee, R. W.; Burns, D. D.; Turner, M. B.; Lokensgard, M. E.; Cooksy, A. L.; Purse, B. W. Electronic Modifications of Fluorescent Cytidine Analogues Control Photophysics and Fluorescent Responses to Base Stacking and Pairing. *Chem. – Eur. J.* **2019**, *25* (5), 1249–1259. https://doi.org/10.1002/chem.201803653.
(26) Schmidt, O. P.; Mata, G.; Luedtke, N. W. Fluorescent Base Analogue Reveals T-Hg II -T Base Pairs Have High Kinetic Stabilities That Perturb DNA Metabolism. *J. Am. Chem. Soc.* **2016**, *138*, 14733–14739. https://doi.org/10.1021/jacs.6b09044.
(27) Saito, Y.; Suzuki, A.; Okada, Y.; Yamasaka, Y.; Nemoto, N.; Saito, I. An Environmentally Sensitive Fluorescent Purine Nucleoside That Changes Emission Wavelength upon Hybridization. *Chem. Commun. Camb. Engl.* **2013**, *49* (50), 5684–5686. https://doi.org/10.1039/c3cc42605j.
(28) Wypijewska del Nogal, A.; Füchtbauer, A. F.; Bood, M.; Nilsson, J. R.; Wranne, M. S.; Sarangamath, S.; Pfeiffer, P.; Rajan, V. S.; El-Sagheer, A. H.; Dahlén, A.; Brown, T.; Grøtli, M.; Wilhelmsson, L. M. Getting DNA and RNA out of the Dark with 2CNqA: A Bright Adenine Analogue and Interbase FRET Donor. *Nucleic Acids Res.* **2020**. https://doi.org/10.1093/nar/gkaa525.
(29) Gardarsson, H.; Kale, A. S.; Sigurdsson, S. Th. Structure–Function Relationships of Phenoxazine Nucleosides for Identification of Mismatches in Duplex DNA by Fluorescence Spectroscopy. *ChemBioChem* **2011**, *12* (4), 567–575. https://doi.org/10.1002/cbic.201000478.
(30) Seo, Y. J.; Ryu, J. H.; Kim, B. H. Quencher-Free, End-Stacking Oligonucleotides for Probing Single-Base Mismatches in DNA. *Org. Lett.* **2005**, *7* (22), 4931–4933. https://doi.org/10.1021/ol0518582.

(31) Shin, D.; Sinkeldam, R. W.; Tor, Y. Emissive RNA Alphabet. *J. Am. Chem. Soc.* **2011**, *133* (38), 14912–14915.
(32) Sandin, P.; Borjesson, K.; Li, H.; Martensson, J.; Brown, T.; Wilhelmsson, L. M.; Albinsson, B. Characterization and Use of an Unprecedentedly Bright and Structurally Non-Perturbing Fluorescent DNA Base Analogue. *Nucl Acids Res* **2008**, *36* (1), 157–167.
(33) Sandin, P.; Wilhelmsson, L. M.; Lincoln, P.; Powers, V. E. C.; Brown, T.; Albinsson, B. Fluorescent Properties of DNA Base Analogue TC upon Incorporation into DNA--Negligible Influence of Neighbouring Bases on Fluorescence Quantum Yield. *Nucl Acids Res* **2005**, *33* (16), 5019–5025.
(34) Rodgers, B. J.; Elsharif, N. A.; Vashisht, N.; Mingus, M. M.; Mulvahill, M. A.; Stengel, G.; Kuchta, R. D.; Purse, B. W. Functionalized Tricyclic Cytosine Analogues Provide Nucleoside Fluorophores with Improved Photophysical Properties and a Range of Solvent Sensitivities. *Chem Eur J* **2014**, *20* (7), 2010–2015.
(35) Dierckx, A.; Miannay, F.-A.; Ben Gaied, N.; Preus, S.; Björck, M.; Brown, T.; Wilhelmsson, L. M. Quadracyclic Adenine: A Non-Perturbing Fluorescent Adenine Analogue. *Chem. - Eur. J.* **2012**, *18* (19), 5987–5997.
(36) Samaan, G. N.; Wyllie, M. K.; Cizmic, J. M.; Needham, L.-M.; Nobis, D.; Ngo, K.; Andersen, S.; Magennis, S. W.; Lee, S. F.; Purse, B. W. Single-Molecule Fluorescence Detection of a Tricyclic Nucleoside Analogue. *Chem. Sci.* **2021**, *12* (7), 2623–2628. https://doi.org/10.1039/D0SC03903A.
(37) Wilhelmsson, L. M.; Sandin, P.; Holmén, A.; Albinsson, B.; Lincoln, P.; Nordén, B. Photophysical Characterization of Fluorescent DNA Base Analogue, TC. *J. Phys. Chem. B* **2003**, *107* (34), 9094–9101.
(38) Turner, M. B.; Purse, B. W. Fluorescent Tricyclic Cytidine Analogues as Substrates for Retroviral Reverse Transcriptases. *ChemPlusChem* **2020**, *85* (5), 855–865. https://doi.org/10.1002/cplu.202000140.
(39) Sillen, A.; Engelborghs, Y. The Correct Use of "Average" Fluorescence Parameters. *Photochem. Photobiol.* **1998**, *67* (5), 475–486. https://doi.org/10.1111/j.1751-1097.1998.tb09082.x.
(40) Sinkeldam, R. W.; Wheat, A. J.; Boyaci, H.; Tor, Y. Emissive Nucleosides as Molecular Rotors. *ChemPhysChem* **2011**, *12* (3), 567–570. https://doi.org/10.1002/cphc.201001002.
(41) Karimi, A.; Börner, R.; Mata, G.; Luedtke, N. W. A Highly Fluorescent Nucleobase Molecular Rotor. *J. Am. Chem. Soc.* **2020**, *142* (34), 14422–14426. https://doi.org/10.1021/jacs.0c05180.
(42) Burns, D. D.; Teppang, K. L.; Lee, R. W.; Lokensgard, M. E.; Purse, B. W. Fluorescence Turn-On Sensing of DNA Duplex Formation by a Tricyclic Cytidine Analogue. *J. Am. Chem. Soc.* **2017**, *139*, 1372–1375. https://doi.org/10.1021/jacs.6b10410.
(43) Bloomfield, V. . A.; Crothers, D. M.; Tinoco, I. *Nucleic Acids; Structures, Properties, and Functions*; University Science Books: Sausolito, CA, 1999.
(44) Wright, D. J.; Force, C. R.; Znosko, B. M. Stability of RNA Duplexes Containing Inosine·cytosine Pairs. *Nucleic Acids Res.* **2018**, *46* (22), 12099–12108. https://doi.org/10.1093/nar/gky907.
(45) Steinbach, P. J.; Ionescu, R.; Matthews, C. R. Analysis of Kinetics Using a Hybrid Maximum-Entropy/Nonlinear-Least-Squares Method: Application to Protein Folding. *Biophys. J.* **2002**, *82* (4), 2244–2255. https://doi.org/10.1016/S0006-3495(02)75570-7.

(46) Sternisha, S. M.; Whittington, A. C.; Martinez Fiesco, J. A.; Porter, C.; McCray, M. M.; Logan, T.; Olivieri, C.; Veglia, G.; Steinbach, P. J.; Miller, B. G. Nanosecond-Timescale Dynamics and Conformational Heterogeneity in Human GCK Regulation and Disease. *Biophys. J.* **2020**, *118* (5), 1109–1118. https://doi.org/10.1016/j.bpj.2019.12.036.
(47) Dickerson, R. E.; Drew, H. R.; Conner, B. N.; Wing, R. M.; Fratini, A. V.; Kopka, M. L. The Anatomy of A-, B-, and Z-DNA. *Science* **1982**, *216* (4545), 475 LP – 485. https://doi.org/10.1126/science.7071593.
(48) Kypr, J.; Kejnovská, I.; Renčiuk, D.; Vorlíčková, M. Circular Dichroism and Conformational Polymorphism of DNA. *Nucleic Acids Res.* **2009**, *37* (6), 1713–1725. https://doi.org/10.1093/nar/gkp026.
(49) Treinin, A.; Hayon, E. Quenching of Triplet States by Inorganic Ions. Energy Transfer and Charge Transfer Mechanisms. *J. Am. Chem. Soc.* **1976**, *98* (13), 3884–3891. https://doi.org/10.1021/ja00429a025.
(50) Shannon, R. D. Revised Effective Ionic Radii and Systematic Studies of Interatomic Distances in Halides and Chalcogenides. *Acta Crystallogr. Sect. A* **1976**, *32* (5), 751–767. https://doi.org/10.1107/S0567739476001551.
(51) Giri, R. Fluorescence Quenching of Coumarins by Halide Ions. *Spectrochim. Acta. A. Mol. Biomol. Spectrosc.* **2004**, *60* (4), 757–763. https://doi.org/10.1016/S1386-1425(03)00287-7.
(52) Guo, Y.; Cao, F.; Qiu, P.; Wang, Z. Studies of the Effect of Halide Ions on the Fluorescence of Quinine Sulfate. *Luminescence* **2019**, *34* (4), 450–455. https://doi.org/10.1002/bio.3627.
(53) Černý, J.; Kabeláč, M.; Hobza, P. Double-Helical → Ladder Structural Transition in the B-DNA Is Induced by a Loss of Dispersion Energy. *J. Am. Chem. Soc.* **2008**, *130* (47), 16055–16059. https://doi.org/10.1021/ja805428q.
(54) Yakovchuk, P.; Protozanova, E.; Frank-Kamenetskii, M. D. Base-Stacking and Base-Pairing Contributions into Thermal Stability of the DNA Double Helix. *Nucleic Acids Res.* **2006**, *34* (2), 564–574. https://doi.org/10.1093/nar/gkj454.
(55) Riley, K. E.; Hobza, P. On the Importance and Origin of Aromatic Interactions in Chemistry and Biodisciplines. *Acc. Chem. Res.* **2013**, *46* (4), 927–936. https://doi.org/10.1021/ar300083h.
(56) Poater, J.; Swart, M.; Bickelhaupt, F. M.; Fonseca Guerra, C. B-DNA Structure and Stability: The Role of Hydrogen Bonding, π–π Stacking Interactions, Twist-Angle, and Solvation. *Org. Biomol. Chem.* **2014**, *12* (26), 4691–4700. https://doi.org/10.1039/C4OB00427B.
(57) Sinkeldam, R. W.; Greco, N. J.; Tor, Y. Polarity of Major Grooves Explored by Using an Isosteric Emissive Nucleoside. *ChemBioChem* **2008**, *9* (5), 706–709. https://doi.org/10.1002/cbic.200700714.

TABLE OF CONTENTS GRAPHIC